nature nanotechnology

LETTERS

PUBLISHED ONLINE: 22 JANUARY 2012 | DOI: 10.1038/NNANO.2011.250

# A local optical probe for measuring motion and stress in a nanoelectromechanical system

Antoine Reserbat-Plantey, Laëtitia Marty, Olivier Arcizet, Nedjma Bendiab and Vincent Bouchiat*

**Nanoelectromechanical systems[1] can be operated as ultrasensitive mass sensors[2,3] and ultrahigh-frequency resonators[4], and can also be used to explore fundamental physical phenomena such as nonlinear damping[5] and quantum effects in macroscopic objects[6]. Various dissipation mechanisms are known to limit the mechanical quality factors of nanoelectromechanical systems and to induce aging due to material degradation, so there is a need for methods that can probe the motion of these systems, and the stresses within them, at the nanoscale. Here, we report a non-invasive local optical probe for the quantitative measurement of motion and stress within a nanoelectromechanical system, based on Fizeau interferometry and Raman spectroscopy. The system consists of a multilayer graphene resonator that is clamped to a gold film on an oxidized silicon surface. The resonator and the surface both act as mirrors and therefore define an optical cavity. Fizeau interferometry provides a calibrated measurement of the motion of the resonator, while Raman spectroscopy can probe the strain within the system and allows a purely spectral detection of mechanical resonance at the nanoscale.**

The outstanding mechanical[7], electrical[8] and optical[9] properties of graphene[10] make it an ideal material for flexible, conductive and semitransparent films. Multilayer graphene contains several tens of atomic layers of carbon, and it is sufficiently stiff[11] to produce freestanding cantilevers with very high aspect ratios that can be used to make suspended mirrors with masses from tens to hundreds of femtograms. Moreover, the optical cavities that are formed when such cantilevers are suspended over a silica surface can be electrostatically actuated, which makes them well suited for the development of nanoelectromechanical systems (NEMS)[12]. Previous attempts to probe the local motion of graphene resonators[13] reached the nanometre scale, but the stress could not be measured directly and only a limited range of pressures and temperatures could be used. However, optical profilometry has recently been employed to probe the static strain in hybrid graphene–metallic cantilevers[14]. In the present work, we use Raman spectroscopy to probe the local stress within a multilayer graphene cantilever. We explore mechanical deformations from d.c. up to megahertz frequencies by taking advantage of the large dynamical resolution of optical detection. Meanwhile, our interferometric approach allows self-calibrated measurements. The displacements measured are considerably larger than those previously reported, and the Raman spectroscopy provides a quantitative analysis of the local stress within the structure.

Samples were prepared from micrometre-sized multilayer graphene planar flakes clamped on one side by a gold film and with overhanging silicon oxide (see Methods). Typical samples had a thickness of ~100 monolayers (~30 nm), as verified by atomic force microscopy (Supplementary Information). Their thicknesses were adjusted to prevent collapse while maintaining semitransparency, with optical reflectance and transmission coefficients of $R = 0.22$ and $T = 0.61$ for 30-nm-thick multilayer graphene[15]. Some flakes tend to stick up after the fabrication process (Fig. 1a) at a wedge angle of $\alpha \in [5^\circ; 35^\circ]$, and these leave a wedge gap of length $h(x, y)$ ranging between 0.3 and 3 μm. The resulting structures form an optical cavity, characterized by a low optical interference order ($n = 2h/\lambda < 10$, where $\lambda$ is the probe wavelength). The top mirror is a deformable multilayer graphene sample of extremely low mass (10–100 fg), exhibiting high mechanical resonance frequencies (1–100 MHz). Among ~100 measured samples, we observed a variety of geometries (Fig. 1), allowing the exploration of various mechanical regimes with a wide range of wedge angles, sizes and shapes. Iridescence was observed under white-light illumination (Fig. 1c), and the interference pattern observed under monochromatic illumination (Fig. 1d) presents contrasted equal-thickness fringes (so-called Fizeau fringes; see Supplementary Information). Unlike conventional graphene-based optical cavities with fixed geometries[16], the optical length of the cavity linearly increases along the cantilever. This allows the observation of multiple interference fringes (Fig. 1c,d). Interference patterns are observed for both the pump laser reflection and Raman scattered light (Supplementary Information). The latter has the considerable advantage of carrying local information related to the material (stress, doping, defects, temperature).

The cavity optical length can also be adjusted by electrostatic actuation of the cantilever, thus producing a translation of the interference fringes pattern (Supplementary Video). This is achieved by applying a d.c. or a.c. voltage $V$ (typically up to 30 V) to the clamp electrode (Fig. 1b) while grounding the $SiO_2$ capped silicon substrate[12]. This results in an attractive electrostatic force $F$, which reduces the cavity length with respect to the equilibrium position $h_0$ in the absence of driving. We measured the response to a harmonic drive, which generated a force quadratic in voltage $F(2\omega) \propto V(\omega)^2$ through local light intensity variations, $\Delta I(x, y, 2\omega, h_0)$:

$$\Delta I(x, y, 2\omega, h_0) \propto \chi_{\mathrm{mec}}(x, y, 2\omega)\chi_{\mathrm{opt}}(x, y, h_0)V(\omega)^2 \qquad (1)$$

where $\chi_{\mathrm{mec}}$ is the mechanical susceptibility (Supplementary Information) and $\chi_{\mathrm{opt}}$ is the optical susceptibility defined as $\chi_{\mathrm{opt}}(x, y, h_0) = \partial g_{\mathrm{opt}}/\partial h$, where $g_{\mathrm{opt}}$ is a periodic interferometric function of $h(x, y)$ defined as the normalized intensity of reflected ($I_r$) or Raman scattered ($I_G$) light: $I_{r,G}/I_0 = g_{\mathrm{opt}}(h)$ (Fig. 1d).

The quadratic dependence of $\Delta I$ on small voltage variations is systematically observed, both for reflected light (Supplementary Fig. S5) and for multilayer graphene Raman lines (Fig. 2a). Because $g_{\mathrm{opt}}$ is $\lambda/2$ periodic, a precise calibration of the low-frequency motion response under electrostatic actuation can be obtained and is found to be of the order of 20 nm $V^{-2}$ (Supplementary Information). We find that the energy of the stress-sensitive optical phonon (so-called Raman G peak) also follows a quadratic dependence with small voltage variations. The

Institut Néel, CNRS et Université Joseph Fourier, BP 166, F-38042 Grenoble Cedex 9, France. *e-mail: vincent.bouchiat@grenoble.cnrs.fr

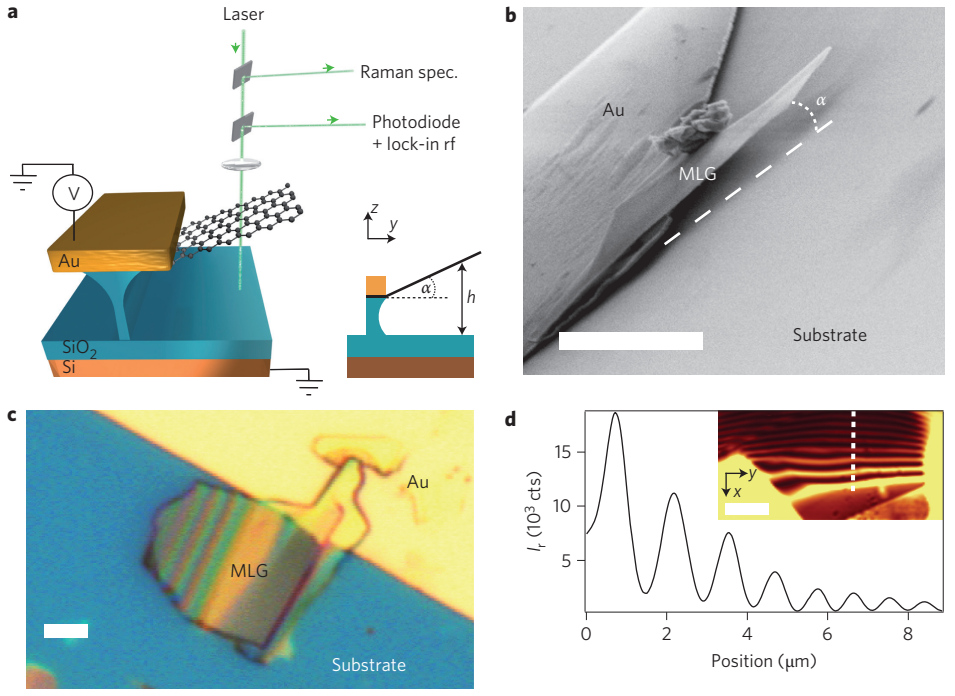


**Figure 1 | Fizeau fringes in a multilayer graphene cantilever. a**, Schematic view of the device. The cantilever can be actuated with an external voltage while its optical properties are analysed with a high-sensitivity Raman spectrometer and a fast photodiode. **b**, Scanning electron micrograph showing a typical multilayer graphene (MLG) cantilever clamped to a gold film on an oxidized silicon substrate. The cantilever and the surface act as an optical cavity because they are both reflecting; light enters and leaves the cavity via the cantilever, which is semitransparent. **c**, White-light optical image of a device showing iridescence. **d**, Reflectance profile measured along the dashed line in the inset. The reduction in signal strength observed at large distances from the hinge is due to reduced spatial mode matching. However, the fringe contrast is preserved. Inset: reflectance confocal ($x$, $y$) scan at 633 nm. Scale bars, 5 μm.

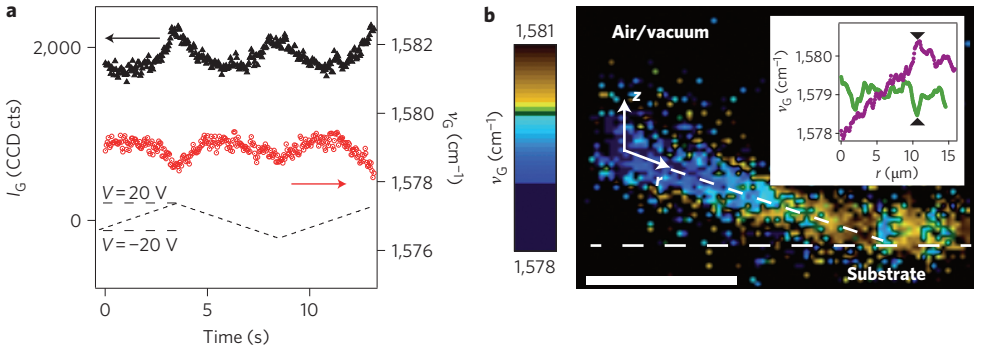


**Figure 2 | Quasistatic actuation and stress mapping of a multilayer graphene cantilever. a**, The intensity $I_G$ (black symbols, left axis) and shift $\nu_G$ (red symbols, right axis) of the Raman G peak of a multilayer graphene cantilever versus time during electrostatic actuation (dashed line). Peak softening can be seen. **b**, False-colour plot showing the value of $\nu_G$ measured during a confocal ($x$, $z$) scan of the cantilever cross-section. The inset shows how $\nu_G$ varies along the cantilever before (purple) and after (green) the collapse of the cantilever onto the silica substrate. Black marks indicate the hinge position. Scale bar, 5 μm.

G peak Raman shift is indeed synchronized with the interferometric response $I_G(t)$ (Fig. 2a), and exhibits softening of ~1.9 $cm^{-1}$ at the maximum cantilever deflection. This Raman peak softening cannot be interpreted as a doping effect because the doping level necessary to induce the observed Raman shifts would correspond to a surface charge much stronger than the one induced by the gate drive[17]. Moreover, the doping induced during a.c. gating would directly follow gate variation and therefore be $\omega$ periodic, which is in disagreement with the observed $2\omega$ Raman shift periodicity (Fig. 2a). This Raman peak softening is interpreted as a stress/strain effect and, by analogy with strained graphene measurements[18–20], it is thus possible to extract a corresponding strain value of 0.06% at maximum deviation resulting from a quasi-static stress of 600 MPa. For such low strain, G-band splitting is not resolved. Also, the stress exerted at the hinge scales as $LF/[W2t^2]$, where $F$, $L$, $W$ and $t$ are the electrostatic force, the cantilever length, width and thickness, respectively (Supplementary Information). For our large-aspect-ratio structures ($L/t \gg 1$), the local stress can be very intense and reaches hundreds of MPa for the electrostatic forces estimated here (~25 nN $\mu m^{-1}$). This value is in agreement with the quasi-static stress of 600 MPa deduced above.

The multilayer graphene Raman signature depends on the position along the flake. A micro-Raman confocal depth scan ($x$, $z$) (Fig. 2b) reveals a linear increase in the position of the G peak along the cantilever axis, from the free end of the cantilever to the hinge, which is not observed when the multilayer graphene is

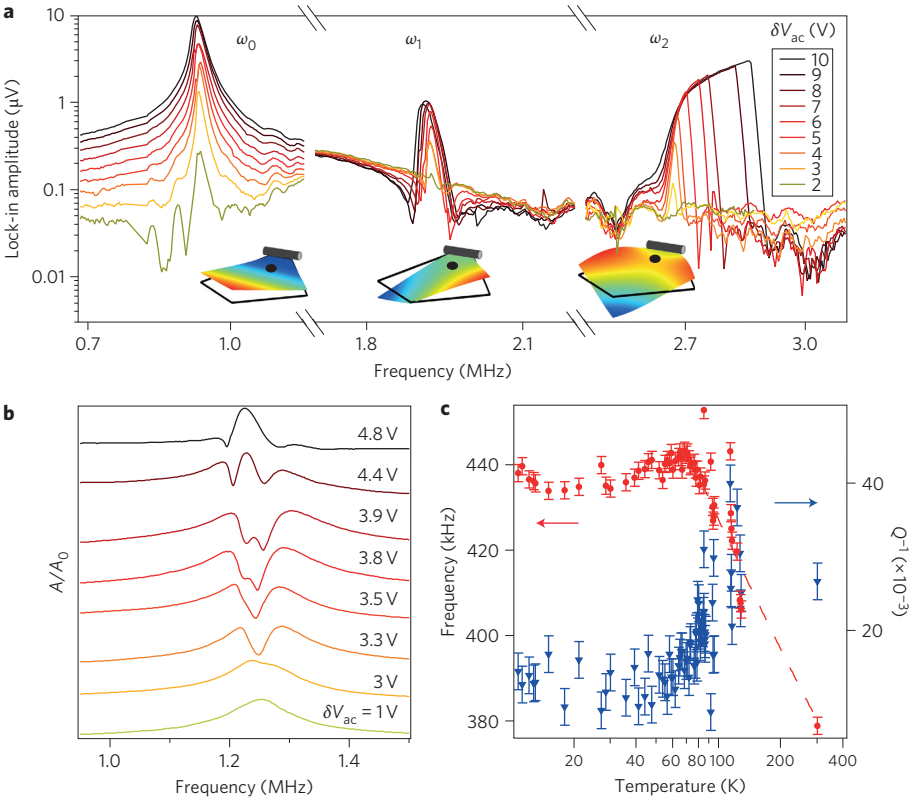


**Figure 3 | Detection of mechanical resonances in multilayer graphene cantilevers by Fizeau interferometry. a**, Amplitude of cantilever oscillations at $2\omega$ (on a logarithmic scale) versus drive frequency for nine different radiofrequency drive voltages showing the nonlinear behaviour of the fundamental mechanical mode ($\omega_0$) and the first two harmonics ($\omega_1$ and $\omega_2$). The schematics show the position of the cantilever at each mode. The black outline shows the position of the cantilever at rest. The black dot shows the position of the laser (which is focused quite close to the hinge). **b**, Amplitude at $2\omega$ (on a linear scale) versus drive frequency for eight drive voltages. The signal folding due to optical interferences can be seen as the drive voltage increases from bottom to top. The laser spot is focused close to the free end of the cantilever. **c**, The resonance frequency (red symbols, left axis) and associated dissipation (blue symbols, right axis) versus temperature of the optical cryostat. Error bars represent s.e.m. Different cantilevers were used for the measurements in **a**,**b** and **c**. All measurements were performed under vacuum and the laser spot was positioned at the edge of a fringe to achieve the optimal values of $\chi_{opt}$.

collapsed (Fig. 2b, inset). This linear shift could be interpreted as a continuously increasing electrostatic field effect[17,21] owing to charge within the substrate, which also influences the position of the Raman G peak[22]. However, in this experiment, the G peak shows local hardening around the hinge position in the suspended case, whereas local softening is observed at the same location after collapse. Indeed, uniaxial strain in multilayer graphene also induces symmetry breaking of the Raman G peak, leading to mode splitting, and each component ($G^+$, $G^-$) softens or hardens under tensile or compressive strain, respectively[7,18]. This stress-induced Raman shift is characterized by an average mode shift rate of about $-3.2\ cm^{-1}\ GPa^{-1}$ (ref. 19). This outcome is in agreement with a maximum compressive strain at the hinge in the suspended case and a transition toward a tensile strain when the cantilever collapses. By converting these Raman shifts into stress at the hinge, this gives an equivalent built-in stress of 300 MPa.

Adjusting both the laser spot position and the drive amplitude allows probing, in a separated fashion, of the nonlinearities arising from mechanical (Fig. 3a) and optical (Fig. 3b) origins. It is worth noting that optical nonlinearities are observed when the probe is far from the hinge (Fig. 3b) where, due to the lever-arm effect, the oscillation amplitude becomes comparable to the probe wavelength. As in the quasi-static regime, it is possible to calibrate the displacement amplitude with respect to the driving excitation $\delta V_{ac}$ by using the periodic nature of $\chi_{opt}$. Peak folding is indeed observed when increasing the drive amplitude above 3 V (Fig. 3b). Assuming a mechanical linear response, the drive increase necessary to produce two successive foldings (corresponding to $\lambda/4$ in amplitude) provides calibration of the drive efficiency, which equals $150\ nm\ V^{-2}$ in the case presented in Fig. 3b. The entire signature of the optical nonlinearities is visible for a restricted range of drive voltage over which no mechanical nonlinearities were observed.

Close to the hinge, optical nonlinearities are extinguished due to smaller variations in $h$, allowing nonlinearities of a mechanical origin to be revealed; these can be observed for larger drive voltages (higher than 4 V; Fig. 3a). This measurement underlines the wide range of mechanical nonlinearities observed in multilayer graphene structures[5,23,24]. It is worth noting that the detection efficiency strongly depends on the mode profile because it is based on Fizeau fringe pattern modulation. $\chi_{mec}(x, y, 2\omega)$ can exhibit important variations along the spatial pattern of the probed vibration. In particular, $\chi_{mec}(x, y, 2\omega)$ can be strongly reduced when the laser probe is focused at a node of the mechanical resonance. As an example, the first harmonic ($\omega_1$), found to be a torsional mode via finite elements analysis, generates a position where the cavity length does not vary (typically, a node region $(x_n, y_n)$). Thus, according to equation(1), $\chi_{mec}(x_n, y_n, 2\omega_1) \ll \chi_{mec}(x_n, y_n, 2\omega_0)$. However, focusing the laser at a different position allows the local optical response to be enhanced. This particular extinction feature of the detection holds great promise for further mapping of multilayer graphene deformation associated with a single mechanical mode.

To investigate the influence of the laser probe in our all-optical method, cryogenic measurements were carried out (Fig. 3c). The

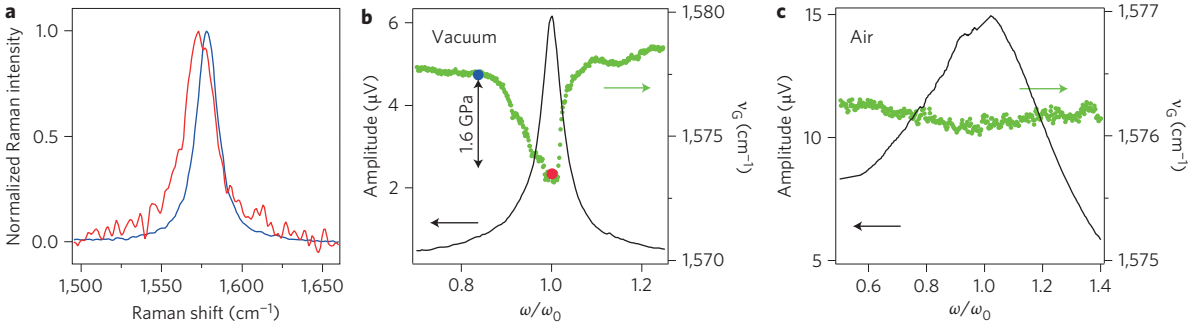


**Figure 4 | Detection of mechanical resonance and dynamic stress using Raman spectroscopy. a**, Raman spectra of the G peak of an electrostatically actuated multilayer graphene cantilever at the mechanical resonance frequency (red) and at a frequency 360 kHz lower than the resonance frequency (blue). The amplitude of the oscillations is higher for the resonant case, which leads to the signal-to-noise ratio being lower than in the off-resonance case because the cantilever spends more time being out of focus. **b**,**c**, Amplitude of cantilever oscillations at $2\omega$ (black line, left axis) and Raman shift (green symbols, right axis) versus drive frequency in vacuum (**b**) and in air (**c**); the radiofrequency drive voltage is 5 V. There is a softening of the G peak at the mechanical resonance frequency, and this softening is more marked under vacuum. Measurements were performed on the same sample as in Fig. 3b. The blue and red symbols in **b** correspond to the Raman spectra shown in Fig. 3.

fundamental resonant frequency exhibits a linear upshift on cooling from 300 K to 70 K, below which it saturates due to extrinsic heating (Supplementary Information). In contrast to doubly clamped graphene-based NEMS[5,12,25], it is not possible to discuss the frequency hardening observed in Fig. 3c in terms of cantilever tensioning induced by differential thermal expansion because we study a simply clamped geometry. An important feature of any resonator is the measurement of the quality factor, defined as $Q = \omega/\Delta\omega$, which characterizes the high sensitivity (high $Q$) of the resonator to its environment. A linear decrease of the ratio of dissipated to stored energy ($Q^{-1}$) is observed on cooling to 70 K. Both effects, frequency hardening and the decrease in dissipation, are possibly a consequence of the stiffening of the clamp electrode. Further measurements will allow us to investigate both extrinsic effects (clamp stiffening losses) and the mechanical intrinsic properties of multilayer graphene, which should bring new insights to understanding the damping mechanisms in NEMS. The effective substrate temperature was obtained by measuring the ratio of the Stokes and anti-Stokes Raman intensities (Supplementary Information), and suggested a temperature threshold of 70 K. All the physical quantities (resonant frequencies, quality factor $Q$, Raman shift) were sensitive to the environmental temperature down to 70 K. This demonstrates experimentally that the room-temperature experiments discussed in this Letter are not altered by laser heating. Regarding the absorption of mechanical energy at resonance, we observed no change in the Raman Stokes/anti-Stokes measurements when sweeping the excitation frequency through the mechanical resonance, indicating no increase in the phonon bath temperature.

To demonstrate the spectral detection of mechanical resonance, the Raman response of the multilayer graphene cantilever was plotted under vacuum (Fig. 4a) at the fundamental mechanical resonance $\omega_0 = 1.2$ MHz (red curve) and off resonance (blue curve). At $\omega_0$, G-peak softening was at a position of $-5\ \mathrm{cm}^{-1}$ with a width of about $+10\ \mathrm{cm}^{-1}$ (full-width at half-maximum (FWHM) of the peak; Fig. 4a), taking into account averaging-induced broadening (Supplementary Information). This Raman softening, estimated at $-1\ \mathrm{cm}^{-1}\ \mathrm{V}^{-2}$, is attributed to a corresponding variation in internal stress, which is enhanced at mechanical resonance according to the universal stress behaviour of $sp^2$ carbon materials[19,20,26] (shift rate, $0.003\ \mathrm{cm}^{-1}\ \mathrm{MPa}^{-1}$). This dynamical stress can therefore be evaluated as ~1.6 GPa, thus providing a quantitative means of detecting NEMS resonance stress effects. It is worth noting that the measured stress in a multilayer graphene cantilever at mechanical resonance is more than one order of magnitude larger than previously reported[27] in silicon-based microelectromechanical system devices.

In Fig. 4b,c, we have detected the fundamental mechanical resonance of this multilayer graphene cantilever using both reflected and Raman scattered light under different experimental conditions. Because the lifetime of optical phonons is much shorter (1 ps) than $\omega_0^{-1}$ (~100 ns), the Raman scattered photons provides instantaneous information related to stress in the vibrating cantilever. For each excitation frequency, we record a Raman spectrum (1 s averaging), which reflects stress at the cantilever position. For several samples, we were able to check that the softening behaviour (Fig. 4b,c, green curve) observed under mechanical excitation coincides with the mechanical resonance width, irrespective of chamber pressure (Fig. 4b,c).

In contrast to the vacuum case (Fig. 4b), where the quality factor was $Q_{vac} \approx 26.1$, the same sample in air (Fig. 4c) presents a reduced quality factor ($Q_{air} = 2.3$) as well as a reduced Raman G-peak softening, which illustrates that locally the dynamical stress is less intense. The value of $Q_{air}$ agrees with a typical viscous damping model[28] for that particular geometry and represents the predominant damping mechanism for limiting the quality factor in air (Supplementary Information). However, this mechanism is no longer dominant under vacuum, where dissipation may be governed by clamping losses. Note that the ratio of the drive efficiency at low frequency ($20\ \mathrm{nm}\ \mathrm{V}^{-2}$) and at resonance ($150\ \mathrm{nm}\ \mathrm{V}^{-2}$) can be compared with the ratio of the G peak shift sensitivity at low frequency ($1\ \mathrm{cm}^{-1}\ \mathrm{V}^{-2}$) and at resonance ($5\ \mathrm{cm}^{-1}\ \mathrm{V}^{-2}$). They are both equal to the measured quality factor $Q$ (~6), as expected for a mechanical resonator[24]. To demonstrate the versatility of the Raman-based spectral detection of the mechanical resonances, we investigated a similar effect on two other types of NEMS (silicon nanocantilevers and SiC nanowires; see Supplementary Information).

We have shown that the variation of the cavity length $h(x, y)$ caused by the displacement of the cantilever generates a mechanical stress that can be determined by measuring the shift in the position of the Raman G peak. Moreover, the strength of the coupling between this shift and the cantilever displacement (which can reach $\sim 1 \times 10^{17}\ \mathrm{Hz\ m}^{-1}$) compares favourably with similar quantities observed in other optomechanical systems[29]. This large optomechanical coupling, in which all the scattered Raman photons carry information on the nanoresonator dynamics, enables (i) mechanical stress information to be spectrally encoded, (ii) an efficient rejection of the background signal, allowing a better signal-to-noise ratio compared to elastic optical detection and (iii) the maintenance of a significant detection of nanosized oscillators, thanks to

the resonant nature of Raman scattering. Similar to experiments in optomechanics[30,31] and atomic physics[32], our work could be used to explore the effects of back-action (due to phonons in our case) in precision measurements.

In conclusion, we demonstrate an optical probe combining Raman spectroscopy with Fizeau interferometry, which provides calibrated mapping of dynamical stress and motion in a NEMS, and enables spectral detection of mechanical resonances. This probe is applied to multilayer graphene NEMS and is fully extendable to other systems (Supplementary Information). Being compatible with cryogenic measurements, it paves the way for stress mapping of high-quality-factor resonators and for the understanding of the dissipation factors that arise at low temperatures. Owing to its stiffness, semitransparency and extremely low mass, multilayer graphene emerges as a platform for the simultaneous exploration of the spatial, temporal and spectral properties of NEMS.

## Methods

Multilayered graphene flakes were deposited on 280-nm-thick oxidized silicon wafer by micro-mechanical exfoliation[10] of Kish graphite. Electrical contacts were made using deep ultraviolet lithography and electron-beam deposition of 50 nm gold film. Samples were suspended by etching (buffered hydrogen fluoride at a concentration ratio of 1:3 $HF/NH_4F$) and drying using $CO_2$ critical point drying. Experiments were performed on ~100 samples (Supplementary Information). Micro-Raman spectroscopy was performed with a commercial Witec Alpha 500 spectrometer set-up with a dual-axis $X$–$Y$ piezo stage in a backscattering/reflection configuration. The grating had 1,800 lines per mm, conferring a spectral resolution of 0.01 $cm^{-1}$ for 10 s integration time. Two laser excitation wavelengths were used: 633 nm (He–Ne) and 532 nm (solid-state argon diode). Raman spectra were recorded in air with a Nikon ×100 objective (NA = 0.9) focusing the light on a 320-nm-diameter spot (532 nm light), and with a Mitutoyo ×50 objective (M plan APO NIR) in vacuum. All measurements made under vacuum (Fig. 3, Fig. 4a,b) were under active pumping at a residual pressure equal to $1 \times 10^{-6}$ bar. For Raman measurements, the laser power was kept below 1 mW $\mu m^{-2}$ and for reflectance measurements below 1 $\mu W\ \mu m^{-2}$. For radiofrequency measurements in air or vacuum, the optical response was recorded with a silicon fast photodiode and a lock-in detector synchronized at twice the radiofrequency drive frequency. The signal was at a maximum when $2\omega_{ac}$ coincided with the fundamental mechanical resonance frequency $\omega_0$ of the cantilever. Cryogenic measurements made use of an optical continuous-helium-flow Janis cryostat with electrical contacts.

Received 1 November 2011; accepted 15 December 2011; published online 22 January 2012

## References


1. Ekinci, K. L. & Roukes, M. L. Nanoelectromechanical systems. *Rev. Sci. Instrum.* **76,** 061101 (2005).
2. Lassagne, B., Garcia-Sanchez, D., Aguasca, A. & Bachtold A. Ultrasensitive mass sensing with a nanotube electromechanical resonator. *Nano Lett.* **8,** 3735–3738 (2008).
3. Jensen, K., Kim, K. & Zettl, A. An atomic-resolution nanomechanical mass sensor. *Nature Nanotech.* **3,** 533–537 (2008).
4. Peng, H. B., Chang, C. W., Aloni, S., Yuzvinsky, T. D. & Zettl, A. Ultrahigh frequency nanotube resonators. *Phys. Rev. Lett.* **97,** 087203 (2006).
5. Eichler, A. *et al.* Nonlinear damping in mechanical resonators based on graphene and carbon nanotubes. *Nature Nanotech.* **6,** 339–342 (2011).
6. O'Connell, A. D. *et al.* Quantum ground state and single-phonon control of a mechanical oscillator. *Nature* **464,** 697–703 (2010).
7. Lee, C., Wei, X., Kysar, J. & Hone, J. Measurement of the elastic properties and intrinsic strength of monolayer graphene. *Science* **321,** 385–388 (2008).
8. Castro Neto, A., Guinea, F., Peres, N. M. R., Novoselov, K. S. & Geim, A. K. The electronic properties of graphene. *Rev. Mod. Phys.* **81,** 109–162 (2009).
9. Nair, R. R. *et al.* Fine structure constant defines visual transparency of graphene. *Science* **320,** 1308 (2008).
10. Novoselov, K. S. *et al.* Electric field effect in atomically thin carbon films. *Science* **306,** 666–669 (2004).
11. Booth, T. J. *et al.* Macroscopic graphene membranes and their extraordinary stiffness. *Nano Lett.* **8,** 2442–2446 (2008).
12. Bunch, S. J. *et al.* Electromechanical resonators from graphene sheets. *Science* **315,** 490–493 (2007).
13. Garcia-Sanchez, D. *et al.* Imaging mechanical vibrations in suspended graphene sheets. *Nano Lett.* **8,** 1399–1403 (2008).
14. Conley, H., Lavrik, N. V., Prasai, D. & Bolotin, K. I. Graphene bimetallic-like cantilevers: probing graphene/substrate interactions. *Nano Lett.* **11,** 4748–4752 (2011).
15. Skulason, H. S., Gaskell, P. E. & Szkopek, T. Optical reflection and transmission properties of exfoliated graphite from a graphene monolayer to several hundred graphene layers. *Nanotechnology* **21,** 295709 (2010).
16. Ling, X. & Zhang, J. Interference phenomenon in graphene-enhanced Raman scattering. *J. Phys. Chem C* **115,** 2835–2840 (2010).
17. Yan, J., Zhang, Y., Kim, P. & Pinczuk, A. Electric field effect tuning of electron-phonon coupling in graphene. *Phys. Rev. Lett.* **98,** 166802 (2007).
18. Otakar, F. *et al.* Compression behavior of single-layer graphenes. *ACS Nano* **4,** 3131–3138 (2010).
19. Otakar, F. *et al.* Development of a universal stress sensor for graphene and carbon fibre. *Nature Commun.* **2,** 255–261 (2011).
20. Huang, M. *et al.* Phonon softening and crystallographic orientation of strained graphene studied by Raman spectroscopy. *Proc. Natl Acad. Sci. USA* **106,** 7304–7308 (2009).
21. Das, A. *et al.* Monitoring dopants by Raman scattering in an electrochemically top-gated graphene transistor. *Nature Nanotech.* **3,** 210–215 (2008).
22. Berciaud, S., Ryu, S., Brus, L. E. & Heinz, T. F. Probing the intrinsic properties of exfoliated graphene: Raman spectroscopy of free-standing monolayers. *Nano Lett.* **9,** 346–352 (2009).
23. Lifshitz, R. & Cross, M. C. Nonlinear dynamics of nanomechanical and micromechanical resonators, in *Review of Nonlinear Dynamics and Complexity* (ed. Schuster, H. G.) (Wiley, 2008).
24. Landau, L. D. & Lifshitz, E. M. *Theory of Elasticity* (Pergamon, 1960).
25. Singh, V. *et al.* Probing thermal expansion of graphene and modal dispersion at low-temperature using graphene nanoelectromechanical systems resonators. *Nanotechnology* **21,** 165204 (2010).
26. Mohiuddin, T. M. G. *et al.* Uniaxial strain in graphene by Raman spectroscopy: G peak splitting, Grüneisen parameters, and sample orientation. *Phys. Rev. B* **79,** 205433 (2009).
27. Pomeroy, J. W. *et al.* Dynamic operational stress measurement of MEMS using time-resolved Raman spectroscopy. *J. Micro. Syst.* **17,** 1315–1321 (2008).
28. Hosaka, H., Itao, K. & Kuroda, S. Damping characteristics of beam-shaped micro-oscillators. *Sens. Actuat. A* **49,** 87–95 (1995).
29. Arcizet, O. *et al.* High-sensitivity optical monitoring of a micromechanical resonator with a quantum-limited optomechanical sensor. *Phys. Rev. Lett.* **97,** 133601 (2006).
30. Anetsberger, G. *et al.* Near-field cavity optomechanics with nanomechanical oscillators. *Nature Phys.* **5,** 909–914 (2009).
31. Anetsberger, G. *et al.* Measuring nanomechanical motion with an imprecision below the standard quantum limit. *Phys. Rev. A* **82,** 1–4 (2010).
32. Kasevich, M. & Chu, S. Laser cooling below a photon recoil with three-level atoms. *Phys. Rev. Lett.* **69,** 1741–1744 (1992).


## Acknowledgements

This work was partially supported by the ANR (MolNanoSpin, Supergraph, Allucinan), ERC (advanced grant no. 226558), and the Nanosciences Foundation of Grenoble. Samples were fabricated in the NANOFAB facility of the Néel Institute. The authors thank A. Allain, D. Basko, C. Blanc, E. Bonet, O. Bourgeois, E. Collin, T. Crozes, L. Del-Rey, M. Deshmukh, E. Eyraud, C. Girit, R. Haettel, C. Hoarau, D. Jeguso, D. Lepoittevin, R. Maurand, J-F. Motte, R. Piquerel, Ph. Poncharal, V. Reita, A. Siria, C. Thirion, P. Vincent, R. Vincent and W. Wernsdorfer for help and discussions.

## Author contributions

A.R.P., N.B. and V.B conceived and designed the experiments. A.R.P., L.M., N.B. and V.B. performed the experiments: A.R.P., O.A., N.B. and V.B. analysed the data. All authors contributed materials/analysis tools. All authors discussed the results and commented on the manuscript.

## Additional information

The authors declare no competing financial interests. Supplementary information accompanies this paper at www.nature.com/naturenanotechnology. Reprints and permission information is available online at http://www.nature.com/reprints. Correspondence and requests for materials should be addressed to V.B.